

## Low-energy positron diffraction from CdTe(110): A minimum-variance $R$ -factor analysis

C. B. Duke, A. Paton, and A. Lazarides

*Xerox Wilson Center of Research & Technology, 800 Phillips Road, 0114-38D, Webster, New York 14580*

D. Vasumathi and K. F. Canter

*The Martin Fisher School of Physics, Brandeis University, Waltham, Massachusetts 02254*

(Received 4 November 1996)

The atomic geometry of the (110) surface of CdTe has been determined by low-energy positron diffraction (LEPD). Diffracted intensities of 13 inequivalent beams were measured at sample temperatures of 110 K over an energy range  $20 \text{ eV} \leq E \leq 140 \text{ eV}$ . These intensity energy profiles were analyzed using a multiple-scattering dynamical theory. The surface structural parameters were determined via a comparison of the calculated and experimentally measured profiles. An uncertainty analysis scheme, expanded from the analogous one proposed for analyses of low-energy electron diffraction intensities, was used to estimate the uncertainties in the structural parameters so as to reflect accurately uncertainties in the measured data. This analysis is based on a minimum-variance least-squares  $R$  factor  $R_{MV}$ , defined and applied to the LEPD data from CdTe(110). It yields the top-layer rotation angle  $\omega_1 = 30.0 \pm 0.5^\circ$ ; the second-layer rotation angle  $\omega_2 = -6.9 \pm 0.2^\circ$ ; and bond lengths  $d(c_2 - a_1) = 2.84 \pm 0.02 \text{ \AA}$ ,  $d(c_1 - a_1) = 2.74 \pm 0.01 \text{ \AA}$ , and  $d(c_1 - a_2) = 2.65 \pm 0.02 \text{ \AA}$ . The uncertainty intervals quoted are the 95% confidence limits ( $\pm 2\sigma$ , where  $\sigma$  is the rms standard deviation) associated with an analysis of the uncertainties in the measured LEPD intensities. Uncertainties in the structural parameters associated with those in the construction of the model of the diffraction process could not be estimated quantitatively. These results agree well with prior structure determinations based on low-energy electron diffraction intensity analysis and x-ray standing waves. They confirm that when measured in units of the bulk lattice constant, the atomic geometry of highly ionic CdTe(110) is comparable to that of the (110) surfaces of other III-V and II-VI semiconductors rather than collapsing to a nearly unrelaxed bulk structure as predicted by an analysis of the role of ionicity on the atomic geometries of the (110) surfaces of zinc-blende structure binary compound semiconductors. [S0163-1829(97)01311-8]

### I. INTRODUCTION

A study of the surface atomic geometry of CdTe(110) by low-energy positron diffraction (LEPD) intensity analysis is of special interest for three reasons. First, surface structure determinations by LEPD, in contrast with low-energy electron diffraction (LEED), intensity analyses are believed to give more accurate surface atomic geometries because of the absence of exchange and the repulsive character of the positron versus electron-ion core interactions.<sup>1,2</sup> For GaAs(110) LEPD and LEED intensity analyses yield essentially identical surface atomic geometries, although for InP(110), the associated surface atomic geometries differ in small but statistically significant ways.<sup>3</sup> A similar result is found for CdSe(10 $\bar{1}$ 0).<sup>4</sup> Thus a study of CdTe(110) was undertaken to assess the nature and extent of these differences. Second, beginning in 1987, Kasowski and co-workers<sup>5-7</sup> revived an earlier notion<sup>8-10</sup> that the zinc-blende (110) surface structures should depend sensitively on ionicity and at high ionicities collapse to slightly relaxed bulklike structures. Although contradicted by several early experimental results<sup>11,12</sup> and subsequent structural studies,<sup>13,14</sup> this notion of ionicity-induced structural collapse seems to live on. Thus the present study of highly ionic (Phillips ionicity<sup>15</sup>  $f_i = 0.72$ ) CdTe(110) by LEPD was undertaken to provide another independent experimental test of its validity. Third and finally, more rigorous uncertainty estimates may be constructed for measured LEPD intensities than for LEED intensities as typically reported because of the details of the digital data collection methodology for weak positron beams.<sup>1,16</sup> This fact, together

with the improved accuracy of models of positron-solid relative to electron-solid interactions,<sup>1,2</sup> offers the opportunity to develop further an uncertainty-analysis methodology<sup>17</sup> that permits uncertainties in the measured intensities due to statistical fluctuations to be propagated directly into corresponding uncertainties of the surface structural parameters extracted from LEPD intensity analysis via an analysis of the local curvature of a suitably chosen  $R$  factor. We develop this extension of Ref. 17 herein during the course of our analysis of LEPD from CdTe(110).

We proceed by describing the experimental data collection and sample preparation in Sec. II. In Sec. III we describe the model calculation of the LEPD intensities for comparison with the measured values. In Sec. IV we describe the structure analysis methodology and in Sec. V the results of its application to CdTe(110). We discuss the significance of these results in Sec. VI.

### II. EXPERIMENTAL PROCEDURES

The apparatus for our LEPD measurements is described in detail elsewhere.<sup>4,18</sup> A major modification of our beam that was made in order to carry out the CdTe(110) LEPD studies with an improved beam flux was to replace our usual W(110) thin-foil transmission moderator<sup>19</sup> with a more efficient solid rare-gas moderator.<sup>20</sup> The emission process in these moderators, discovered by Gullikson and Mills,<sup>21</sup> is different from metal moderators where the positron thermalizes rapidly and is subsequently remitted from a negative work-function material. In the rare-gas solid, once the positron energy is less than the band gap, energy loss by electron-hole pair creation

is no longer possible. The positron continues to lose energy by creating phonons, but the maximum phonon energy is small and therefore the diffusion length for the “hot positrons” is large, resulting in a higher reemission efficiency. Solid Ne has been found to have the highest reemission efficiency among the rare-gas solids.<sup>21</sup>

In our system we are able to produce a primary beam of 200 000 slow positrons per second with our 31-mCi primary positron source: a factor of 5 increase in flux over our previous W(100) foil moderator. As welcome as this increase in flux is, we pay a price in the deliverable angular spread and beam size on target. Rare-gas moderators emit nonthermal positrons, resulting in an emission angular distribution that is approximately three times wider than the 10° spread typical of W(100) foil moderators.<sup>18</sup> Since our rare-gas moderator consists of argon condensed on a 4-mm-diam source spot, as opposed to our previous 6-mm-effective-diam W(100) foil moderator, however, we obtain an on-target deliverable beam with a diameter angular spread product, i.e., the reciprocal of the beam emittance, that is approximately twice that of the 1-mm-rad product (at 30 eV) using the W(100) foil moderator. We accommodated the poorer emittance by doubling the size of beam incident on the sample to ~1.5 mm at 30 eV, for example. This allowed us to keep the incident angular spread to within  $\pm 1^\circ$ . The concession in beam diameter, but not in angular spread, results in no degradation of the resolution of the features of the diffraction intensity versus incident energy curves (the  $I$ - $V$  profiles) while allowing one to take full advantage of the increase in flux offered by the solid argon moderator.

The primary positron source, deposited on a 4-mm spot and covered with a thin 5- $\mu\text{m}$  Ti window, is mounted on a second stage of a closed cycle refrigerator that could be cooled to ~15 K. Ar is condensed directly on the cold source to form the moderator. The fast positrons from <sup>22</sup>Na are moderated in their energy by the solid Ar and subsequently undergo two stages of reflection mode remoderation from Ni(100) so as to enhance the beam brightness. Elastically diffracted positrons from the sample surface pass through a hemispherical retarding field analyzer and are detected by a two-dimensional (2D) position-sensitive detector. The position of any detected positron is digitized to address a memory location in a 2D buffer. The counts in the selected memory address are then incremented by 1, yielding a 2D histogram that comprises the diffraction pattern. Computer control was used to set the incident beam energy, focus the beam onto the sample surface, enable the 2D buffer to accumulate data for a chosen interval, read the diffraction data from the 2D buffer, and store the data as a file on hard disk.<sup>3</sup>

Quantitative LEED measurements also were performed on CdTe(110) using the same LEPD diffractometer. A heated W filament located behind the last remoderation cathode aperture emitted a copious number of electrons that were then transported to the sample using the same optics as the positrons but with reversed polarities of the power supplies. The electron beam produced in this way has a poorer emittance (approximately a factor of 2 times larger) than the remoderated positron beam and far less than that of commercial LEED guns. As for positrons, the larger spot size does not degrade that resolution of the features of the LEED  $I$ - $V$  profiles. We do not analyze these data further because they

are essentially identical to those used in earlier structural studies.<sup>22</sup>

CdTe(110) crystals were obtained from Cleveland Crystals.<sup>23</sup> These had typical resistivities  $\sim 10^6 \Omega \text{ cm}$ . Each crystal was a bar  $5 \times 5 \times 25 \text{ mm}^3$  with the (110) surface being the  $5 \times 5 \text{ mm}^2$  face. A pair of adjacent faces were the (001) face. Grooves 50  $\mu\text{m}$  deep were cut on this (001) face to facilitate cleaving. The samples were then mounted on a thin oxygen-free high-conductivity copper holder, with a high thermal and electrical conductivity silver epoxy. This was then mounted on a manipulator sample mount that was coupled to a liquid-nitrogen (LN<sub>2</sub>) reservoir via a copper braid. Using this arrangement, the sample could be cooled to a temperature of 100 K. An electrostatic mirror was mounted on the manipulator but rotated 90° from the sample. This mirror reflected the positrons back to the diffractometer with an efficiency of 64% and was used to determine the incident flux for normalization of the diffracted intensities.

The crystals were cleaved *in situ*. Good defect-free large areas  $\sim 3 \times 3 \text{ mm}^2$  were typically obtained from the cleaves as seen in display LEED maps of the surface. Normal incidence of the positron beam was ensured by checking the symmetry of the diffraction pattern [the ( $hk$ ) spot is equivalent to the ( $\bar{h}\bar{k}$ ) spot] for normal incidence. The bulk Debye temperature  $\Theta_D$  for CdTe is 200 K.<sup>24</sup> Even at the low measurement temperatures of 100 K, the fairly high  $\Theta_D$  leads to a substantial reduction in diffracted intensities, the effect being greater at higher energies. This leads to very low diffracted intensities beyond 130 eV. Therefore, an energy range between 10 and 140 eV was chosen for the LEPD measurements. The range was divided into two: (i) 10–60 eV in 2-eV steps since most of the structure in the  $I$ - $V$  profiles were found in this region and (ii) 50–140 eV in steps of 4 eV. The overlapping energies served as a check on beam stability and beam normalization.<sup>3</sup>

Six separate autosequences were run over the energy range of interest so that statistically significant data could be obtained. Every autosequence consisted of 30–40 diffraction patterns at definite energy steps. A typical diffraction pattern at 75 eV is shown in Fig. 1. From the raw diffraction pattern, the intensity of each spot and the corresponding background were calculated using a procedure described by Chen *et al.*<sup>3</sup> This was done over the entire autosequence to obtain the spot intensity as a function of energy, i.e., the  $I$ - $V$  profile. In this way, each autosequence was analyzed individually. To get the final experimental data, equivalent spots in each autosequence were averaged using weighted average methods after ensuring that the  $I$ - $V$  profiles for equivalent spots were indeed equivalent. Then the data for all autosequences were averaged again.<sup>3</sup> The final LEPD  $I$ - $V$  profiles from CdTe(110) for 13 nonequivalent beams were used for structure analysis.

In order to verify that the experimental  $I$ - $V$  profiles had sufficient statistics to make an accurate structure determination, we calculated a “self-x-ray factor”  $R_x^{\text{self}}$ , which measures only the contribution of the statistical fluctuations to the  $R_x$  value that will correspond to the actual structure analysis.<sup>16</sup> For the LEPD data taken with about 1 h per energy point,  $R_x^{\text{self}}$  was calculated to be 0.005. Typically, a 0.02 variation in  $R_x$  is considered to be sufficient to distinguish between structures.<sup>3</sup> Thus, for the experimental LEPD data from CdTe(110), it can be concluded that statistics would not

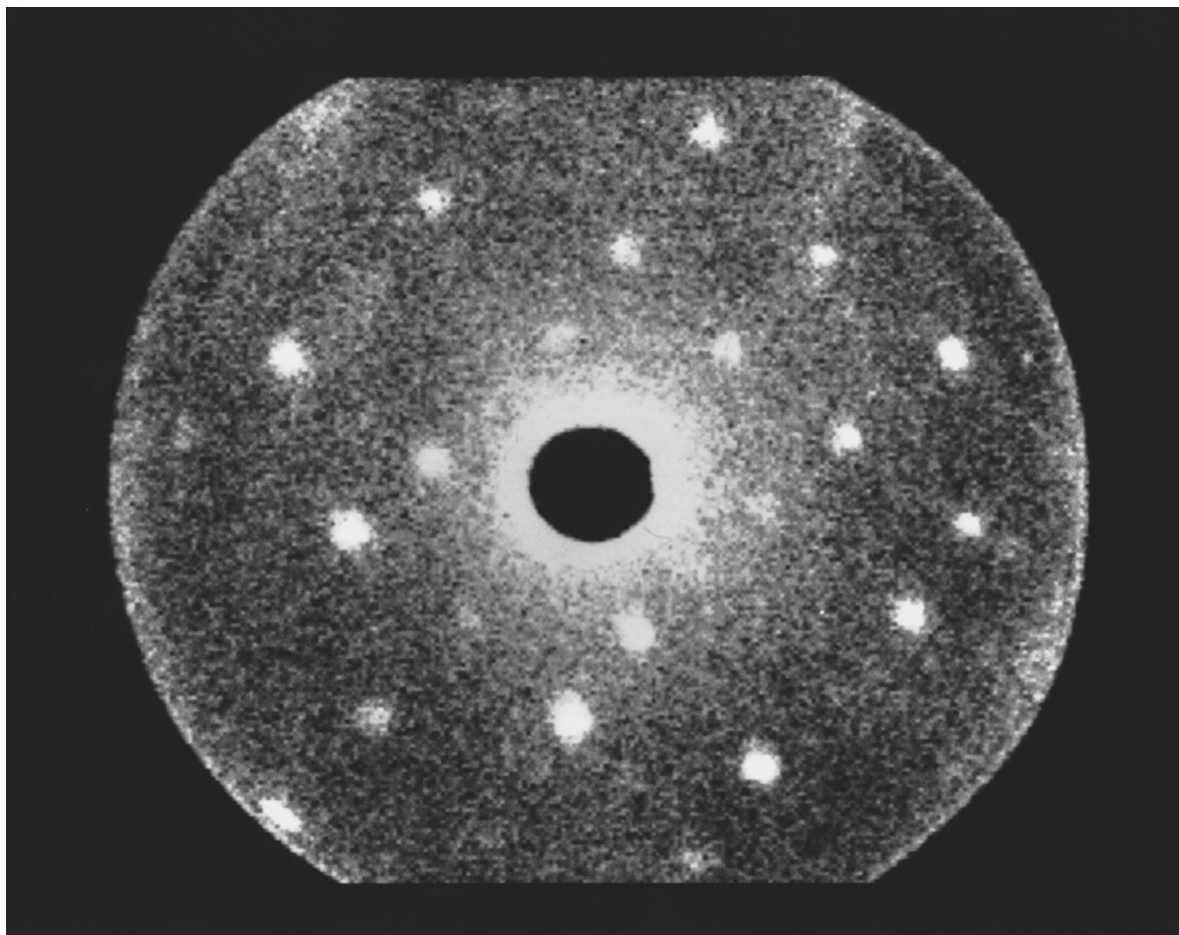


FIG. 1. Low-energy positron diffraction pattern at 75 eV.

be a limiting factor in the determination of an accurate surface structure. A more quantitative statement of how the statistical fluctuations in the measured data propagate into the statistical uncertainties of the structural parameters determined from the data is described in the remainder of this paper. The LEPD experiments were repeated on four different cleaves to check for reproducibility of  $I$ - $V$  profiles. The data from separate cleaves were reproducible within statistical uncertainties, typically 1% per data point.

### III. MODEL CALCULATIONS

The LEPD data were analyzed using the multiple-scattering model of Duke and Laramore,<sup>25,26</sup> which is a generalization of an analysis of Beeby<sup>27</sup> to include thermal vibrations of the ion cores and complex values of the electron or positron self-energies. A comprehensive review of the theory and its application to LEPD has been given recently by Duke.<sup>2</sup> Charged-particle scattering by crystal ion cores is described by energy-dependent phase shifts that are calculated from the potential distribution experienced by the scattering particle. This potential is approximated by a muffin-tin form calculated from the potential and charge distributions of isolated atoms, which are obtained from a relativistic self-consistent Hartree-Fock-Slater calculation.<sup>28</sup> A  $\rho^{1/3}$  exchange term is used in calculating the isolated atomic potentials. To obtain the crystal potential, these atomic potentials are super-

posed with bulk crystal coordination using the muffin-tin approximation. This potential is then inserted into a radial Schrödinger equation, which is integrated to give the scattering wave phase shifts. The inner potential  $V_0$  between the muffin-tins relative to the vacuum is taken to be an adjustable parameter in the fitting procedure. The major differences in the scattering potential seen by the positrons are in the sign of the Coulomb term and the absence of the exchange term.<sup>29</sup> The positron phase shifts from Cd and Te are shown in Fig. 2. All calculations were performed using six phase shifts. The effect of the thermal vibrations was not considered explicitly in calculating the LEPD intensities.

In the multiple-scattering calculations, the semi-infinite crystal is replaced by a slab of 12 bilayers (12 layers each of Cd and Te). A complete analysis of the multiple scattering is done for the outer eight bilayers, with contributions from the next four bilayers to the scattering amplitudes computed individually and added to the scattering amplitudes from the eight outer bilayers. Two attenuation models were used for the LEPD structure analysis: the constant  $V_i$  model, where  $V_i$  is the imaginary part of the self-energy and the Oliva model.<sup>30</sup> The computer program used was an adaptation of that described by Meyer *et al.*<sup>31</sup>

A schematic diagram of the structural parameters of the zinc-blende (110) surfaces is shown in Fig. 3. Five independent structural parameters were chosen to be optimized via a comparison of the calculated and measured  $I$ - $V$  profiles.

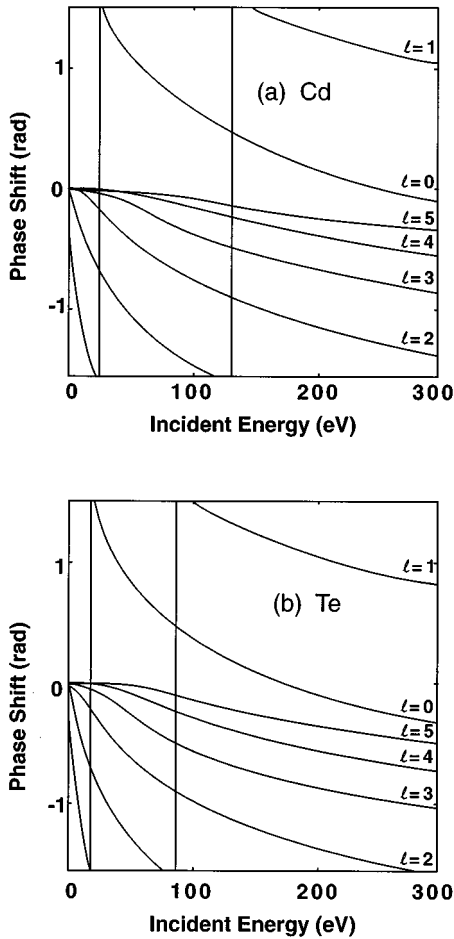


FIG. 2. Rigid lattice positron phase shifts in radians for (a) Cd and (b) Te.

These were  $\omega_1$  and  $\omega_2$ , the chain tilt angles in the first and second layers, respectively, and  $c_2 - a_1$ ,  $c_1 - a_1$  and  $c_1 - a_2$ , where  $c_i - a_j$  indicates the bond length between the cation in layer  $i$  and the anion in layer  $j$ . Third and deeper layers atoms are assumed to be at their bulk positions.  $V_0$ , the offset of the internal energy zero, also was taken to be an adjustable parameter to be optimized by fitting the measured intensities.

#### IV. STRUCTURE ANALYSIS

The present LEPD structure analysis differs from its predecessors<sup>3,32</sup> for zinc-blende (110) surfaces in three respects. First, since bond length changes are expected for the ionic II-VI compounds,<sup>3,33</sup> we utilize bond lengths and tilt angles directly as the independent structural variables<sup>34,35</sup> as indicated in Fig. 3. Second, since we are providing an uncertainty analysis based on the statistics of experimentally recorded counts, we utilize the Gaussian  $R$  factor  $R'_2$ , defined and discussed by Duke *et al.*<sup>17</sup> as the figure of merit determining the goodness of fit between the calculated and measured intensity profiles. For purposes of comparison with prior results, we also give the values of the x-ray<sup>4,36</sup> and integrated intensity<sup>37</sup>  $R$  factors used previously. Third, since the data acquisition process described in Sec. II leads to an independent uncertainty assessment  $\sigma_{hk}(E_i)$  for each inten-

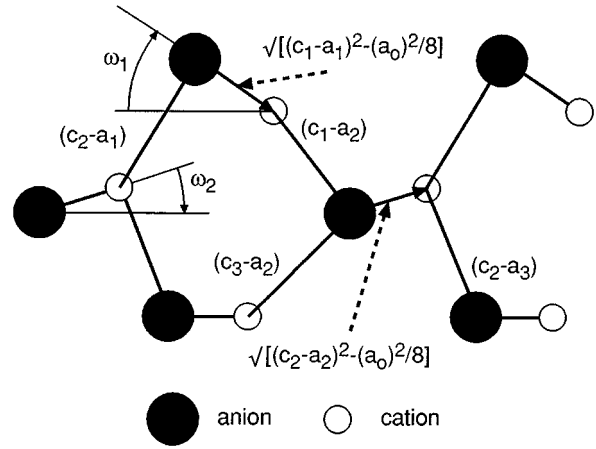


FIG. 3. Planar side-view projection of the zinc-blende (110) surfaces illustrating the independent surface structural parameter expressed as bond lengths  $c_i - a_j$  and chain tilt angles  $\omega_i$ . The symbol  $c_i - a_j$  designates the bond length between the cation in the  $i$ th layer and the anion in the  $j$ th layer.  $\omega_i$  designates the tilt angle (relative to the unrelaxed surfaces) of the planar zigzag chains in the  $i$ th layer.

sity data point, we extend  $R'_2$ , which assumes that all the data points have the same  $\sigma_{hk}(E_i)$ , to incorporate this additional information. This leads us to define an extended version of  $R'_2$ , labeled by  $R_{MV}$ , as described below. We evaluate “best-fit” structures by minimizing separately both  $R'_2$  and  $R_{MV}$  and compare the results.

The structure analysis proceeds by first minimizing the normalized Gaussian  $R$  factor<sup>17,38,39</sup>

$$R'_2 = (FI_{av}^2)^{-1} \sum_{h,k} \sum_i [cI_{hk}^{\text{theory}}(E_i) - I_{hk}^{\text{expt}}(E_i)]^2, \quad (1a)$$

$$F = n - p - 1, \quad (1b)$$

$$c = N/D, \quad (1c)$$

$$N = \sum_{h,k} \sum_i [I_{hk}^{\text{theory}}(E_i) I_{hk}^{\text{expt}}(E_i)], \quad (1d)$$

$$D = \sum_{h,k} \sum_i [I_{hk}^{\text{theory}}(E_i)]^2, \quad (1e)$$

$$I_{av}^2 = n^{-1} \sum_{h,k} \sum_i [I_{hk}^{\text{expt}}(E_i)]^2, \quad (1f)$$

$$n = \sum_{h,k} n_{hk} \quad (1g)$$

as a function of the  $p$  independent parameters (structural and nonstructural) that are to be determined by fitting the intensity data. The  $n_{hk}$  are the number of data points in the  $(hk)$  beam so that  $n$  is the total number of data points in the sample. (For example, if multiple angles of incidence are used in the data sample, they also would be summed over to get  $n$ .) We perform this step via an automated search routine<sup>34,35</sup> using the downhill simplex method.<sup>40</sup> At its completion we obtain an estimate of the best-fit structure. In

general, this estimate depends both on the starting structure and on the parameters included in the simplex. Consequently, one must verify the identification of a global minimum by using multiple starting structures and parameter sets.

As described by Duke *et al.*,<sup>17</sup>  $R'_2$  defined by Eqs. (1) is appropriate when every intensity measurement  $I_{hk}^{\text{expt}}(E_i)$  is characterized by the same Gaussian error distribution of mean zero and variance  $\sigma_e^2 \cong I_{av}^2 R'_2(\text{min})$  and the errors at different values of  $(hk)$  and  $E_i$  are uncorrelated. In the case that the errors for the various values of  $(hk)$  and  $E_i$  remain uncorrelated but the measurement points exhibit Gaussian distributions with different variances, a more appropriate<sup>17,39</sup>  $R$  factor is the minimum-variance  $R$  factor  $R_{\text{MV}}$ , given by

$$R_{\text{MV}} = F^{-1} \sum_{h,k} \sum_i [c' I_{hk}^{\text{theory}}(E_i) - I_{hk}^{\text{expt}}(E_i)]^2 / \sigma_{hk}^2(E_i), \quad (2a)$$

$$c' = N' / D', \quad (2b)$$

$$N' = \sum_{h,k} \sum_i [I_{hk}^{\text{theory}}(E_i) I_{hk}^{\text{expt}}(E_i)] / \sigma_{hk}^2(E_i), \quad (2c)$$

$$D' = \sum_{h,k} \sum_i [I_{hk}^{\text{theory}}(E_i) / \sigma_{hk}(E_i)]^2. \quad (2d)$$

Since the data analyses procedure described in Sec. II yields different values of  $\sigma_{hk}(E_i)$  for different values of  $(hk)$  and  $E_i$ , we use these values directly in Eqs. (2) to define  $R_{\text{MV}}$ , which we then minimize to obtain an optimal structure. The inverse variance weighting of the terms in the  $R_{\text{MV}}$  sum tends to drive the structure search to structures with intensities that match the lower variance data points more closely than the higher variance data points. The low weighting assigned to high variance data constrains the effect on the structural results of data noise to a lower level than in the case of the uniform variance  $R$  factor  $R'_2$ . If uncertainties associated with the calculation of intensities (i.e., model uncertainties) are small relative to data uncertainties and if the data uncertainties are properly assigned, the minimum-variance  $R$  factor  $R_{\text{MV}}$  should lead to a structure with uncertainty levels (variances) that are lower than those of structures derived using other figures of merit.

Uncertainty levels for the various parameters are calculated as a group from the curvature of the  $R$ -factor surface in the vicinity of the global minimum using matrix methods that account for correlations among parameter estimation errors. The  $R$ -factor curvature matrix is defined as the second-order coefficient matrix in a second-order expansion of the Gaussian  $R$  factor about its minimum as a function of the  $p$  parameters to be determined, i.e.,

$$R(\mathbf{a}) = R_0 + (\mathbf{a} - \mathbf{a}_{\text{est}})^t \left[ \frac{1}{2} \frac{\partial^2 R'_2}{\partial \mathbf{a}^2} \right]_0 (\mathbf{a} - \mathbf{a}_{\text{est}}), \quad (3a)$$

$$(\mathbf{a} - \mathbf{a}_{\text{est}})^t = [(a_1 - a_{1,\text{est}}), \dots, (a_p - a_{p,\text{est}})]. \quad (3b)$$

$R_0$  is the minimum values of  $R$  at the global minimum defined by

$$\mathbf{a}_{\text{est}} = [a_{1,\text{est}}, \dots, a_{p,\text{est}}], \quad (3c)$$

in which the  $a_i$  must include the independent structural parameters but also may include nonstructural parameters as well (typically  $V_0$ , but also  $\lambda_{ee}$ ,  $\langle u^2 \rangle$ , and  $X_\alpha$  if desired). In these equations  $R$  can be either  $R'_2$  or  $R_{\text{MV}}$ . The variances  $\sigma_i^2$  in the (Gaussian) distributions of model parameters caused by uncorrelated, Gaussian distributed uncertainties in the individual intensity values  $I_{hk}(E_i)$  are given by the diagonal terms of the covariance matrix

$$[\text{cova}] = \frac{2R'_{20}}{F} \left[ \frac{\partial^2 R'_2}{\partial^2 \mathbf{a}} \right]_0^{-1}, \quad (4a)$$

$$[\text{cova}]_{ii} = \sigma_i^2 \quad (4b)$$

[see Eq. (12b) of Ref. 17] for  $R'_2$ , whereas for  $R_{\text{MV}}$  Eq. (4a) is replaced by [Eq. (26a) of Ref. 17]

$$[\text{cova}] = \frac{2}{F} \left[ \frac{\partial^2 R_{\text{MV}}}{\partial^2 \mathbf{a}} \right]_0^{-1} \quad (4c)$$

because  $R'_{20}$  is an estimate of  $\sigma_e^2$  that is divided out in the definition of  $R_{\text{MV}}$ . The diagonal terms describe the total variance associated with all the variables in the  $p$ -dimensional vector  $\mathbf{a}$  and hence they tend to increase as more parameters are included in  $\mathbf{a}$ . For example, inclusion of the nonstructural parameters increases the variances associated with the structural parameters in those cases in which the two are correlated (provided, of course, uncorrelated random noise in the measurements is the only source of error). These correlations are assessed by examining the correlation matrix

$$P_{ij} = [\text{cova}]_{ij} / \sigma_i \sigma_j. \quad (5)$$

In the case of the fitting experimental data the inclusion of more nonstructural parameters in  $\mathbf{a}$  may or may not increase the variances of the structural parameters depending upon whether the residual errors are due primarily to measurement errors or to systematic errors in the model.

We performed the error analysis numerically by fitting the quadratic form [similar to Eq. (3a) but including a nonzero gradient term] to the  $R'_2(\mathbf{a})$  or  $R_{\text{MV}}(\mathbf{a})$  surfaces in the vicinity of the value  $\mathbf{a}_{\text{est}}$  located by the simplex search. This code is described by Duke *et al.*<sup>17</sup> Once this form is determined, an improved set of values for  $\mathbf{a}_{\text{est}}$  is obtained from its minimum and the associated elements of the curvature matrix  $[\partial^2 R / \partial \mathbf{a}^2]_0$  in Eq. (3a) are determined. Inversion of the curvature matrix yields the covariance matrix [see Eq. (4) and the following paragraph], which is converted to the correlation matrix using Eq. (5).

## V. RESULTS

$I$ - $V$  profiles for 13 nonequivalent beams were used to determine the structure for CdTe(110). These are  $(01)$ ,  $(0\bar{1})$ ,  $(02)$ ,  $(0\bar{2})$ ,  $(03)$ ,  $(10) = (\bar{1}0)$ ,  $(11) = (\bar{1}\bar{1})$ ,  $(1\bar{1}) = (\bar{1}1)$ ,  $(12) = (\bar{1}2)$ ,  $(20) = (20)$ ,  $(21) = (21)$ ,  $(2\bar{1}) = (2\bar{1})$ , and  $(2\bar{2}) = (2\bar{2})$ . For this data set, simplex searches were initiated and allowed to continue until the spread in each of the five structural parameters among the simplex vertices was smaller than 0.005 Å. Two sets of data were used: the complete set for 20 eV  $\leq E_i \leq 134$  eV and a reduced set over the energy range 40 eV  $\leq E_i \leq 134$  eV. This was done both because of the onset at

TABLE I. Unrelaxed, best-fit structures from analyses of LEPD data and previously determined structures for CdTe(110). In the top row, superscript 1 indicates that the value of  $a_0$  is that used by Duke *et al.* (Ref. 22) as well as in this paper. Superscript 2 (second-row) indicates that the value of  $a_0$  is that used by Cowell and Carvalho (Ref. 41). Superscript 3 (third row) designates the LEED best-fit structure found by Duke *et al.* (Ref. 22). Superscript 4 (fourth row) designates the LEED best-fit structure found by Cowell and Carvalho (Ref. 41). Superscript 5 (fifth row) designates the XSW best-fit structure found by Kendelewicz *et al.* (Ref. 14). Superscript 6 (sixth row) designates the theoretical FP LMTO structure predicted by Kendelewicz *et al.* (Ref. 14) scaled by the ratio of the observed (row 2) to the predicted bulk lattice constant. Superscript 7 (seventh row) indicates the best-fit structure, using  $R'_2$ , 20–134 eV. Superscript 8 (eighth row) indicates the best-fit structure, using  $R_{MV}$ , 20–134 eV. Superscript 9 (ninth row) indicates the best-fit structure, using  $R'_2$ , 40–134 eV. Superscript 10 (tenth row) indicates the best-fit structure, using  $R_{MV}$ , 40–134 eV. Angles are measured in degrees, bond lengths in angstroms and voltages in eV. NA denotes that calculation of this quantity is not appropriate.

$a_0$	$\omega_1$	$\omega_2$	$c_2 - a_1$	$c_1 - a_1$	$c_1 - a_2$	$V_0$	$V_1$	$R'_2$	$R_x$	$R_{xg}$	$R_1$	$R_{MV}$
6.480	0 <sup>1</sup>	0	2.806	2.806	2.806	5.17	4.457	0.796	0.335	0.533	0.670	NA
6.482	0 <sup>2</sup>	0	2.807	2.807	2.807	5.12	4.457	0.796	0.334	0.533	0.671	NA
6.480	30.5 <sup>3</sup>	-6.34	2.680	2.807	2.829	0.00	4.457	0.143	0.114	0.182	0.099	NA
6.482	30.5 <sup>4</sup>	-3.32	2.925	2.809	2.629	0.58	4.457	0.142	0.102	0.211	0.122	NA
6.482	28.7 <sup>5</sup>	0	2.807	2.807	2.807	0.00	4.457	0.172	0.147	0.254	0.122	NA
6.482	29.5 <sup>6</sup>	-0.46	2.802	2.741	2.676	1.64	4.457	0.142	0.123	0.218	0.124	NA
6.480	29.6 <sup>7</sup>	-6.75	2.815	2.730	2.663	1.66	4.457	0.098	0.073	0.120	0.094	NA
6.480	30.1 <sup>8</sup>	-6.68	2.835	2.746	2.665	0.95	4.457	NA	0.073	0.122	0.092	26.5
6.480	29.5 <sup>9</sup>	-7.02	2.855	2.735	2.644	0.97	4.457	0.120	0.101	0.125	0.088	NA
6.480	30.5 <sup>10</sup>	-7.04	2.845	2.744	2.635	1.45	4.457	NA	0.089	0.124	0.088	15.6

$E_i \leq 40$  eV of large new inelastic channels that are not well described by our model of the inelastic damping<sup>2,32</sup> and because the reduced coordination at the surface can exert a significant effect on the phase shifts of the scatterers in the uppermost one or two layers in this energy range. Hence we do not expect the model to describe the measured intensities as well as for  $E_i$  below 40 eV: an expectation borne out by the results. The structures obtained using the two energy ranges are consistent within the uncertainty estimates, however, a fortunate occurrence that we could not have predicted since model uncertainty is the main source of discrepancy between the measured and calculated intensities for  $E_i \leq 40$  eV, and we do not incorporate the influence of this uncertainty explicitly in our analysis. Once the simplex search had converged for each data set, we fit a quadratic representation to the  $R$ -factor surface in the vicinity of the simplex structure, as described in Sec. IV, and used this surface to obtain both the final best-fit structure and the curvature matrix  $\partial^2 R / \partial^2 \mathbf{a}$  used to evaluate the covariance matrix and the correlation matrix.

The resulting best-fit structures obtained from both  $R'_2$  and  $R_{MV}$  are given in Table I together with comparisons with the results of prior structure determinations for CdTe(110) by LEED,<sup>22,41</sup> x-ray standing waves<sup>14</sup> (XSW's), and a first-principles theoretical prediction of the structure reported by Kendelewicz *et al.*<sup>14</sup> The top two rows of Table I show the results for the unreconstructed structure for the two different values of the bulk lattice constant used in the literature. Evidently their differences in describing the data are insignificant and hence are ignored in the discussion that follows. All of our results are obtained using  $a_0 = 6.480$  Å, as indicated in row 1 of Table I. For each of the four best-fit structures reported in rows 7–10 of Table I, the associated rms structural parameter deviations are given in Tables II–V and correlation matrices are given in Tables VI–IX, respectively. The intensity profiles of the best overall fit to the intensity data as measured by  $R_{MV}$  are shown in Fig. 4. Visual com-

parisons of all four best-fit structures with the measured intensity data are essentially indistinguishable from each other.

## VI. DISCUSSION

As evident from Table I, the structures for CdTe(110) obtained by our four LEPD analyses are very nearly identical and are comparable to earlier ones found by LEED (Refs. 22 and 41) and XSW (Ref. 14) analyses. Moreover, except for small changes in the top-layer bond lengths, they differ little from that obtained by initial LEED intensity analysis<sup>22</sup> reported in 1981. Moreover, our LEED data are fully compatible with the data used in this analysis. Therefore, our LEPD intensity analysis provides further support for the notion that increasing ionicity generates small changes in the surface bond lengths but not a wholesale collapse of the approximately universal (110) surface structure of zinc-blende structure binary semiconductors. Moreover, no systematic discrepancy occurs between the values of the tilt angles  $\omega_1$  and  $\omega_2$  found by the LEED and LEPD structures, just as in the case of GaAs. This indicates that LEED and LEPD yield similar results for binary compound semiconductors when both constituents lie in the same row of the Periodic Table: a result that suggests that large differences in atomic scattering

TABLE II. Standard deviations for the structure in row 7 of Table I.

Parameter	$\sigma$
$\omega_1$	0.470
$\omega_2$	0.386
$c_2 - a_1$	0.021
$c_1 - a_1$	0.009
$c_1 - a_2$	0.023
$V_0$	0.156

TABLE III. Standard deviations for the structure in row 8 of Table I.

Parameter	$\sigma$
$\omega_1$	0.069
$\omega_2$	0.050
$c_2 - a_1$	0.003
$c_1 - a_1$	0.002
$c_1 - a_2$	0.003
$V_0$	0.030

TABLE IV. Standard deviations for the structure in row 9 of Table I.

Parameter	$\sigma$
$\omega_1$	0.655
$\omega_2$	0.285
$c_2 - a_1$	0.016
$c_1 - a_1$	0.010
$c_1 - a_2$	0.017
$V_0$	0.034

TABLE V. Standard deviations for the structure in row 10 of Table I.

Parameter	$\sigma$
$\omega_1$	0.119
$\omega_2$	0.063
$c_2 - a_1$	0.004
$c_1 - a_1$	0.003
$c_1 - a_2$	0.004
$V_0$	0.060

TABLE VI. Correlation matrix for the structure in row 7 of Table I.

Parameter	$\omega_1$	$\omega_2$	$c_2 - a_1$	$c_1 - a_1$	$c_1 - a_2$	$V_0$
$\omega_1$	1	-0.008	0.239	-0.703	0.261	-0.244
$\omega_2$		1	-0.139	0.113	-0.018	0.086
$c_2 - a_1$			1	-0.061	-0.718	-0.270
$c_1 - a_1$				1	-0.445	-0.090
$c_1 - a_2$					1	-0.034
$V_0$						1

TABLE VII. Correlation matrix for the structure in row 8 of Table I.

Parameter	$\omega_1$	$\omega_2$	$c_2 - a_1$	$c_1 - a_1$	$c_1 - a_2$	$V_0$
$\omega_1$	1	-0.059	0.386	-0.773	0.235	-0.071
$\omega_2$		1	-0.184	0.124	-0.052	0.169
$c_2 - a_1$			1	-0.257	-0.600	-0.291
$c_1 - a_1$				1	-0.399	-0.146
$c_1 - a_2$					1	-0.028
$V_0$						1

TABLE VIII. Correlation matrix for the structure in row 9 of Table I.

Parameter	$\omega_1$	$\omega_2$	$c_2 - a_1$	$c_1 - a_1$	$c_1 - a_2$	$V_0$
$\omega_1$	1	0.028	0.379	-0.879	0.467	-0.011
$\omega_2$		1	-0.005	0.050	-0.055	-0.001
$c_2 - a_1$			1	-0.336	-0.499	-0.018
$c_1 - a_1$				1	-0.563	-0.007
$c_1 - a_2$					1	-0.036
$V_0$						1

factor between these two constituents, which occur in LEED but not LEPD, cause the systematic differences between the resulting structures observed for InP(110) (Ref. 3) and CdSe(1010).<sup>4</sup>

An important dimension of the results concerns the compatibility of the structures specified in Table I. The structural parameters derived using  $R'_2$  and those derived using  $R_{MV}$  and the reduced data set differ from the structural parameters derived using  $R_{MV}$  and the full data set (line 8 of Table I) by more than  $2\sigma_i$  (Table III). That is, the alternative structures (lines 7, 9, and 10) thus lie outside the 95% confidence region of the minimum-variance structure obtained using the complete data set. For the two structures determined using  $R'_2$  as a figure of merit, the deviations can be attributed to improper weighting of the residuals  $I^{\text{expt}} - cI^{\text{theory}}$ . The equal weights lead to inadequate use of low-variance data and overuse of high-variance data. The lack of overlap between the 95% confidence regions of the large and small data set  $R_{MV}$  structures (lines 8 and 10 of Table I) is small, failing only for  $\omega_2$  and  $c_1 - a_2$ . Nevertheless, it suggests that the covariances calculated for these structures are too small and that the assumptions that govern the validity of Eq. (4c) are not fully satisfied. The assumption of negligible model uncertainty is clearly suspect, even for positrons, although we have no way at present to estimate its effects reliably. Notwithstanding the differences between  $R'_2$  and  $R_{MV}$  we can render all of our results consistent by assigning the structural variables and 95% confidence limits according to

$$\omega_1 = 30.0 \pm 0.5^\circ, \quad (6a)$$

$$\omega_2 = -6.9 \pm 0.2^\circ, \quad (6b)$$

$$d(c_2 - a_1) = 2.84 \pm 0.02 \text{ \AA}, \quad (6c)$$

TABLE IX. Correlation matrix for the structure in row 10 of Table I.

Parameter	$\omega_1$	$\omega_2$	$c_2 - a_1$	$c_1 - a_1$	$c_1 - a_2$	$V_0$
$\omega_1$	1	0.013	0.535	-0.896	0.263	0.287
$\omega_2$		1	-0.136	0.060	-0.210	0.330
$c_2 - a_1$			1	-0.507	-0.346	-0.092
$c_1 - a_1$				1	-0.329	-0.354
$c_1 - a_2$					1	-0.227
$V_0$						1

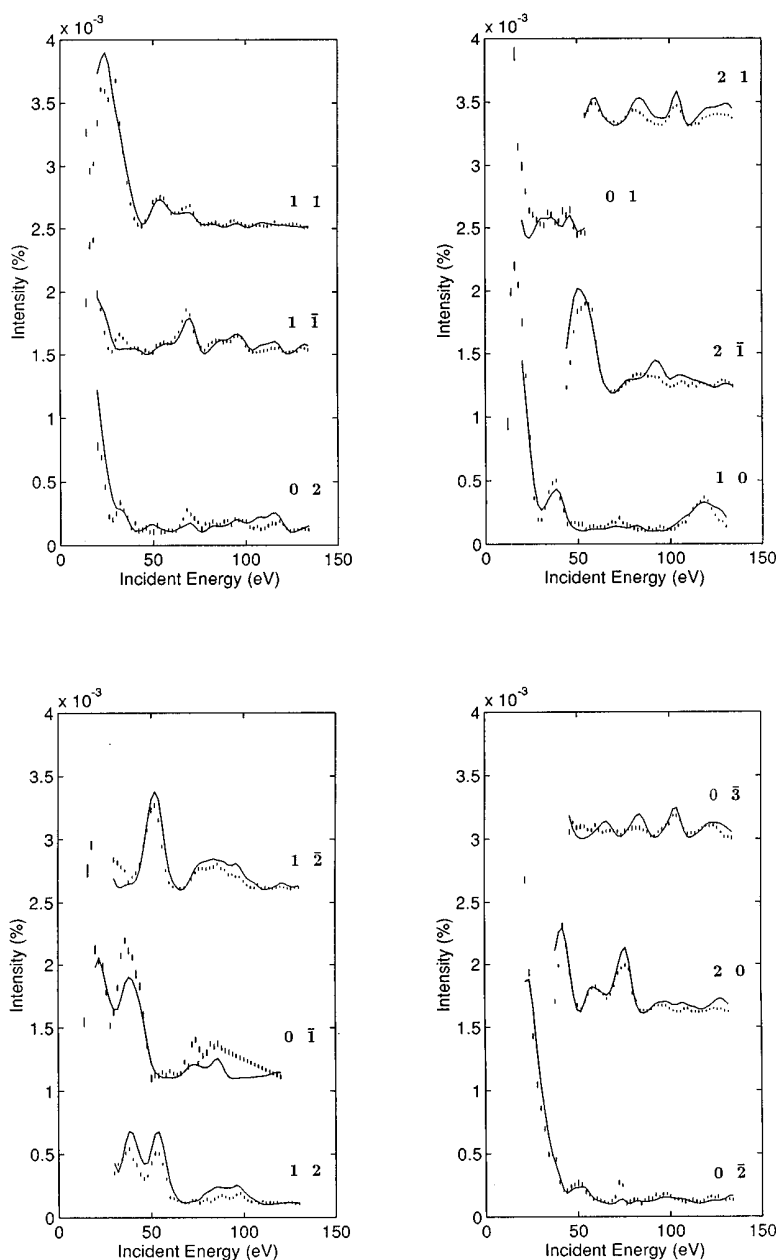


FIG. 4. LEPD experimental  $I$ - $V$  profiles compared with those predicted by the theoretical model that minimizes  $R_2'$  over the entire  $20 \text{ eV} \leq E_i \leq 134 \text{ eV}$  data range.

$$d(c_1 - a_1) = 2.74 \pm 0.01 \text{ \AA}, \quad (6d)$$

$$d(c_1 - a_2) = 2.65 \pm 0.02 \text{ \AA} \quad (6e)$$

as an overall estimate of the accuracy of our structural results due to data uncertainties alone. Using these uncertainties, we can conclude that  $c_1 - a_1$  and  $c_1 - a_2$  are clearly contracted relative to their bulk value of  $2.81 \text{ \AA}$ . Establishing this sort of accuracy for small bond length changes was one of the major goals of the uncertainty analysis methodology developed by Duke *et al.*<sup>17</sup> A comparison of the best-fit results (rows 7–10, Table I) with a bond-length-conserving rotation (row 5, Table I) and the prior LEED structures (rows 3 and 4, Table I) reveals clearly that the small changes in bond length obtained using our fitting software on the LEPD intensity data significantly improves the quality of the model description of these data. Nevertheless, we need to keep in mind that

consideration of model uncertainties will certainly expand the size of the uncertainty ranges given in Eq. (6).

The uncertainty analysis methodology also illustrates another desirable feature of minimum-variance methods. A frequently raised issue in the analysis of low-energy positron or electron diffraction intensities is that of selecting the appropriate data energy range. The greater difficulty of matching theory and experiment at the lower energy ranges of LEED and LEPD data (due to challenges posed both by the theory and by experiment) makes the prospect of including low-energy data in the analysis appear somewhat unreliable. The concern is that due to uncertainties in the model, as well as the data, the structural results may become less, not more, accurate, which is a likely possibility when low-energy residuals are weighted as heavily as mid-range residuals. It is our hypothesis that information contained in low-energy data can be used constructively if it is weighted properly. We tested this hypothesis by comparing the error levels calcu-

lated for the  $R_{MV}$  structure derived from 20–134 eV data with the error levels calculated for the structure derived from 40–134 eV data. All six parameters had smaller  $\sigma$ 's when the full data set was used, suggesting that the weights built into  $R_{MV}$  allowed for successful incorporation of the higher variance low-energy information. In contrast, a comparison of the uncertainties associated with the  $R'_2$  structures revealed that five of six parameters had *greater* uncertainties when the full data set was used. The value of the low-energy data is therefore lost when the low-energy data is weighted as heavily as the mid-range data.  $R'_2$  is thus shown to be a less useful figure of merit when the residuals are of uneven variance.

## VII. SYNOPSIS

In this paper we report LEPD intensity measurements for CdTe(110) and their analysis using a statistically significant

$R$  factor  $R_{MV}$  to determine its surface atomic geometry. The resulting surface structure closely resembles that obtained by prior LEED intensity analyses,<sup>22,41</sup> but exhibits different values for the surface bond lengths relative to the results of those analyses. It further reveals that the surface structure of CdTe(110) is very similar to that of the (110) surfaces of other III-V and II-VI binary semiconductors, thereby contradicting the notion<sup>5–7</sup> that the (110) surface structures of highly ionic compound semiconductors collapse to slightly distorted bulk atomic geometries.

## ACKNOWLEDGMENTS

We would like to acknowledge important suggestions of D. L. Lessor in running some of the codes used in the diffraction calculations and for his active collaboration in early stages of this work. This work was supported in part by the National Science Foundation, Grant No. DMR-88203450.

- 
- <sup>1</sup>K. F. Canter, C. B. Duke, and A. P. Mills, Jr., in *Chemistry and Physics of Solid Surfaces VIII*, edited by R. Vanselow and R. Howe (Springer-Verlag, Berlin, 1990), p. 183.
- <sup>2</sup>C. B. Duke, in *Positron Spectroscopy of Solids*, Proceedings of the International School of Physics "Enrico Fermi," Course CXXV, Varenna, 1993, edited by A. Dupasquier and A. P. Mills, Jr. (IOS, Amsterdam, 1995), p. 317.
- <sup>3</sup>X. M. Chen, K. F. Canter, C. B. Duke, A. P. Mills, Jr., D. L. Lessor, and W. K. Ford, *Phys. Rev. B* **48**, 2400 (1993).
- <sup>4</sup>T. N. Horsky, G. R. Brandes, K. F. Canter, C. B. Duke, A. Paton, A. Kahn, S. F. Horng, K. Stevens, K. Stiles, and A. P. Mills, Jr., *Phys. Rev. B* **46**, 7011 (1992).
- <sup>5</sup>R. V. Kasowski, M.-H. Tsai, and J. D. Dow, *J. Vac. Sci. Technol. B* **5**, 953 (1987).
- <sup>6</sup>M.-H. Tsai, J. D. Dow, R. P. Wang, and R. V. Kasowski, *Superlatt. Microstruct.* **6**, 431 (1989).
- <sup>7</sup>M.-H. Tsai, J. D. Dow, R. P. Wang, and R. V. Kasowski, *Phys. Rev. B* **40**, 9818 (1989).
- <sup>8</sup>C. B. Duke, A. R. Lubinsky, and P. Mark, *J. Vac. Sci. Technol.* **13**, 761 (1976).
- <sup>9</sup>C. B. Duke, *Crit. Rev. Solid State Mater. Sci.* **8**, 69 (1978).
- <sup>10</sup>C. B. Duke, R. J. Meyer, and P. Mark, *J. Vac. Sci. Technol.* **17**, 971 (1980).
- <sup>11</sup>C. B. Duke, *J. Vac. Sci. Technol. A* **10**, 2032 (1992).
- <sup>12</sup>C. B. Duke, in *Festkörperprobleme/Advances in Solid State Physics*, edited by R. Helbig (Vieweg, Braunschweig/Wiesbaden, 1994), vol. 33, p. 1.
- <sup>13</sup>A. Kahn, S. Ahsan, W. Chen, M. Dumas, C. B. Duke, and A. Paton, *Phys. Rev. Lett.* **68**, 3200 (1992).
- <sup>14</sup>T. Kendelewicz, J. E. Klepeis, J. C. Woicik, S. H. Southworth, C. Mailhiot, M. van Schilfgaarde, M. Methfessel, A. Herrara-Gomez, and K. Miyano, *Phys. Rev. B* **51**, 10 774 (1995).
- <sup>15</sup>J. C. Phillips, *Bonds and Bands in Semiconductors* (Adaemic, New York, 1973).
- <sup>16</sup>K. F. Canter, in *Positron Spectroscopy of Solids* (Ref. 2), p. 385.
- <sup>17</sup>C. B. Duke, A. Lazarides, A. Paton, and Y. R. Wang, *Phys. Rev. B* **52**, 14 878 (1995).
- <sup>18</sup>K. F. Canter, G. R. Brandes, T. N. Horsky, P. H. Lippel, and A. P. Mills, Jr., in *Atomic Physics with Positrons*, edited by J. W. Humberston and E. A. G. Armour (Plenum, New York, 1987), p. 153.
- <sup>19</sup>D. M. Chen, K. G. Lynn, R. Pareja, and B. Nielsen, *Phys. Rev. B* **31**, 4123 (1985).
- <sup>20</sup>D. Vasumathi, G. Amarendra, K. F. Canter, and A. P. Mills, Jr., *Appl. Surf. Sci.* **85**, 154 (1995).
- <sup>21</sup>E. M. Gullikson and A. P. Mills, Jr., *Phys. Rev. Lett.* **57**, 376 (1986).
- <sup>22</sup>C. B. Duke, A. Paton, W. K. Ford, A. Kahn, and G. Scott, *Phys. Rev. B* **24**, 3310 (1981).
- <sup>23</sup>Cleveland Crystals, Cleveland, OH 44110.
- <sup>24</sup>A. Kahn, *Surf. Sci. Rep.* **3**, 193 (1983).
- <sup>25</sup>C. B. Duke and G. E. Laramore, *Phys. Rev. B* **2**, 4765 (1970).
- <sup>26</sup>G. E. Laramore and C. B. Duke, *Phys. Rev. B* **5**, 267 (1972).
- <sup>27</sup>J. L. Beeby, *J. Phys. C* **1**, 82 (1968).
- <sup>28</sup>W. K. Ford, C. B. Duke, and A. Paton, *Surf. Sci.* **112**, 195 (1985).
- <sup>29</sup>C. B. Duke and D. L. Lessor, *Surf. Sci.* **225**, 81 (1990).
- <sup>30</sup>J. Oliva, *Phys. Rev. B* **21**, 4909 (1981).
- <sup>31</sup>R. J. Meyer, C. B. Duke, A. Paton, A. Kahn, E. So, J. L. Yeh, and P. Mark, *Phys. Rev. B* **19**, 5194 (1979).
- <sup>32</sup>D. L. Lessor, C. B. Duke, X. M. Chen, G. R. Brandes, K. F. Canter, and W. K. Ford, *J. Vac. Sci. Technol. A* **10**, 2585 (1992).
- <sup>33</sup>D. L. Lessor, C. B. Duke, A. Kahn, and W. K. Ford, *J. Vac. Sci. Technol. A* **11**, 2205 (1993).
- <sup>34</sup>W. K. Ford, T. Guo, D. L. Lessor, and C. B. Duke, *Phys. Rev. B* **42**, 8952 (1990).
- <sup>35</sup>W. K. Ford, T. Guo, K.-J. Wan, and C. B. Duke, *Phys. Rev. B* **45**, 11 896 (1992).
- <sup>36</sup>E. Zanazzi and F. Jona, *Surf. Sci.* **62**, 61 (1977).
- <sup>37</sup>C. B. Duke, S. L. Richardson, A. Paton, and A. Kahn, *Surf. Sci.* **127**, L135 (1983).
- <sup>38</sup>A. A. Lazarides, C. B. Duke, A. Paton, and A. Kahn, *Phys. Rev. B* **52**, 14 895 (1995).
- <sup>39</sup>W. Menke, *Geophysical Data Analysis: Discrete Inverse Theory* (Academic, San Diego, 1989), pp. 58–60.
- <sup>40</sup>W. H. Press, S. A. Teukolsky, W. T. Vetterling, and B. P. Flannery, *Numerical Recipes in Fortran* (Cambridge University Press, Cambridge, 1992), pp. 402–404.
- <sup>41</sup>P. G. Cowell and V. E. de Carvalho, *J. Phys. C* **21**, 2983 (1988).